A FREQUENCY RESPONSE BASED STRUCTURAL DAMAGE LOCALIZATION METHOD USING PROPER ORTHOGONAL DECOMPOSITION

M. Salehi [*] **S. Ziaei-Rad** [**] **M. Ghayour** [***]

Department of Mechanical Engineering
Isfahan University of Technology
Isfahan, 84156-83111, Iran

M.A. Vaziri-Zanjani [****]

Department of Aerospace Engineering
Amirkabir University of Technology
Tehran, Iran

ABSTRACT

Vibration-based structural damage detection has been the focus of attention by many researchers over the last few decades. However, most methods proposed for this purpose utilize extracted modal parameters or some indices constructed based on these parameters. A literature review revealed that few papers have employed Frequency Response Functions (FRFs) for detecting structural damage. In this paper, a technique is presented for damage detection which is based on measured FRFs. Proper Orthogonal Decomposition (POD) has been implemented on spatiotemporal responses in each frequency in order to reduce the dimension of the data. This is based on the concept that the forced harmonic response of a linear vibrating system can be fully captured utilizing a single basis vector. A different approach is also presented in this paper in which POD is applied to the frequency domain data. Operational Deflection Shapes (ODSs) have been decomposed using POD to localize the damage. The efficiency of the method is demonstrated through some numerical and experimental case studies.

Keywords : Damage-Frequency Response Function-Proper Orthogonal Decomposition.

1. INTRODUCTION

Vibration-based damage detection methods are non-destructive global approaches which are based on the fact that any stiffness reduction in a structure affects its dynamic characteristics. Wide range practical applications of vibration-based structural damage detection in aerospace structures, bridges, civil infrastructures, and mechanical systems have attracted the attention of many researchers over the past few decades. All these methods are based on variations in structural dynamic properties caused by the damage. Sohn *et al*. [1] has reviewed most of the research carried out in this area. According to the process of treating the measured data, the vibration- based damage detection methods can be classified into model-based and non-model-based methods. The former identify damage by comparing an analytical model representing the healthy structure and the experimental data from the corresponding damaged structure [2]. However, development of a precise finite element model is usually difficult due to inherent deficiencies and errors in finite element modeling [3].

In the non-model-based damage detection methods, the differences in modal parameters between the intact and damaged states of the structure are directly used or correlated with other relevant information to develop damage indicators for localizing damage. Early works of damage index methodology made use of natural frequency and mode shape data. Shifts in natural frequencies [4]; changes in modal assurance criteria, or MAC [5]; changes in the co-ordinate modal assurance criterion, or COMAC [6]; and changes in the multiple damage location assurance criterion, or MDLAC [7] between the intact and damaged structures are typically used in these methods for localizing damage. Pandey *et al*. [8] demonstrated that changes in mode shape curvature could be a good indicator of damage, particularly for beam-like structures.

A wide variety of non-model-based methods utilize modal parameters extracted from Frequency Response Functions (FRFs). Generally, modal parameters involving spatial data, such as mode shapes, result in a more robust detection. However, experimentally extracted mode shapes are unfortunately often uncertain and inaccurate [9], causing these methods to be less effective.

[*] Graduate student, corresponding author [**] Professor [***] Associate Professor [****] Assistant Professor

DOI : 10.1017/jmech.2011.17
Copyright © 2011 The Society of Theoretical and Applied Mechanics, R.O.C.
https://doi.org/10.1017/jmech.2011.17 Published online by Cambridge University Press

Perhaps, Maia *et al*. were one of the first to apply the FRF data directly to damage detection problems [10]. They extended the mode shape curvature method to all frequencies in the measurement range rather than just to modal frequencies. A 10 DOFs lumped mass model was then used to study the effects of frequency range, input force location, and noise on the method [11]. Liu *et al*. made use of the residual imaginary part of FRF shapes to locate the structural damage [12]. They applied Gapped Smoothing Method (GSM) as well as Wavelet Transform (WT) to locate the abnormality caused by the damage in a cantilever finite element model of a beam. The results were satisfactory over a wide frequency range.

Adhikari and Friswell applied Karhunen-Loeve Decomposition (KLD) and eigensensitivity analysis to update distributed parameters of finite element models [13]. Feeny and Kappagantu related Proper Orthogonal Modes (POMs) to Linear Normal Modes (LNMs) of vibrating systems. They concluded that, in a discrete undamped vibrating system, POMs achieved through POD of free vibration responses converged to LNMs [14]. Feeny and Liang presented a framework to extract structural modal parameters using POD of time responses of structures [15]. The main advantage of this method over the frequency domain modal analysis methods is that it does not require the exciting input force to be measured. The main drawback of POD-based modal extraction method, however, is that the mass matrix has to be known a priori. Chelidze and Zhou improved the KLD-based modal extraction method through Smooth Orthogonal Decomposition (SOD) [16]. They overcame the above-mentioned drawback of POD.

Galvanetto *et al*. applied KLD decomposition to structural damage detection, making use of proper orthogonal decomposition of the forced responses of two numerical beam models at some specific frequencies [17]. In a subsequent paper, they published the experimental verification of their proposed method applied to a cantilever beam [18].

Trendafilova *et al*. used POD and pattern recognition to distinguish the categories of damaged and healthy wing data. They used a modified Principal Component Analysis (PCA) method which reduced the dimensionality of FRFs and made the PCA transformed data more differentiable from the two healthy and damaged categories [19].

There is a close relationship between POD and Singular Value Decomposition (SVD) in the sense that POMs are left singular vectors of the snapshot matrix of the data gathered. Each column of a snapshot matrix is the vector of discrete time histories of measured values of the corresponding sensor. In most practical algorithms for POD, SVD is implemented as an efficient mathematical tool. Lower singular values usually correspond to less important principal directions [20,21].

In this paper, POD is employed to locate the structural damage using FRF data as input. Two approaches are introduced here. In the first approach, FRFs are utilized to construct spatiotemporal matrices of the response data at each frequency. Then, POD is carried out on healthy and damaged state response data to localize damage via GSM. In the second approach, operating deflection shapes in the frequency domain are subjected to POD in order to reveal the damaged zone.

The rest of the paper is organized as follows: Section 2 reviews the POD related formulations. Section 3 summarizes the formulation and properties of FRF shapes. The proposed structural damage detection techniques are described in Section 4. Finally, the proposed method is verified through one numerical and two experimental case studies.

2. PROPER ORTHOGONAL DECOMPOSITION

Given m time samples for each of n measurement points of a vibrating structure, the observation matrix $X_{n\times m}$ can be constructed. Columns of matrix X, called snapshots, are the deflection shapes of the structure at the corresponding moment. The main objective in POD is to find a reduced order data matrix $X_{n\times p}$ ($p < m$) whose columns are an optimal orthonormal basis vector set. By optimal basis is meant a basis with the maximum data set projection on it.

The observation matrix X is formed as follows:

$$X = \begin{bmatrix} x(t_1) & x(t_2) & \cdots & x(t_m) \end{bmatrix} = \begin{bmatrix} x_1(t_1) & x_1(t_2) & \cdots & x_1(t_m) \\ x_2(t_1) & x_2(t_2) & \cdots & x_2(t_m) \\ \vdots & \vdots & \ddots & \vdots \\ x_n(t_1) & x_n(t_2) & \cdots & x_n(t_m) \end{bmatrix} \tag{1}$$

where, $x(t_i)$ is the snapshot at time t_i and the subscript of x stands for the sensor number. The means are often subtracted from the column vectors of X when performing POD.

Two POD computational methods, namely SVD-based and covariance methods, are introduced below.

The SVD of matrix X can be performed as:

$$X = U\Sigma V^T \tag{2}$$

where, $U_{n\times n}$ is an orthonormal matrix containing POM vectors of data, $\Sigma_{n\times m}$ is a matrix with zero off-diagonal elements, and $V_{m\times m}$ is an orthonormal matrix whose rows are the time coefficients of the corresponding POM.

In the second method, called covariance method, the covariance matrix of zero-meaned data is written as:

$$C = \frac{1}{m} XX^T \tag{3}$$

Since C is a real and symmetric matrix, its eigenvectors are orthogonal. It can be proved that eigenvectors and eigenvalues of C are POMs and POVs, respectively [22].

Proper Orthogonal Values (POVs) provide a measure of the amount of participation of the corresponding modes in the data. Amongst the criteria defined to

https://doi.org/10.1017/jmech.2011.17 Published online by Cambridge University Press

decide about the number of dominant POVs, the following is commonly used for choosing the smallest POV index p [17]:

$$\frac{\sum_{i=1}^{p}\lambda_i}{\sum_{i=1}^{N}\lambda_i} \geq c \tag{4}$$

in which, c is a constant number near unity, namely 0.9999. In the case of noisy data, c should be properly selected so as to minimize the effect of noise on the reconstructed data.

POD provides an efficient way of capturing dominant components of measured response data using a few POMs. POMs contain more energy per identified mode than any other decomposition due to its optimality. Moreover, POVs indicate energy content of each mode, *i.e.* its significance in the reconstruction of the original data.

In the case of forced harmonic vibration of linear systems, the response is captured by a single POM [23] where all LMNs contribute to the response. This property can be used to treat structural damage considering vibration data packed in a single vector of POM rather than all LNMs.

3. FRF SHAPES OF VIBRATING SYSTEMS

The FRF of an n DOF system with structural damping, whose excitation and response are measured at DOFs k and j, respectively, is given by [24]

$$\alpha_{jk}(\omega) = \frac{x_j}{f_k} = \sum_{r=1}^{n} \frac{\phi_{jr}\,\phi_{kr}}{\omega_r^2 - \omega^2 + i\eta_r\,\omega_r^2} \tag{5}$$

in which, ϕ_{jr} is the j^{th} element of the r^{th} structural mode shape, ω_r is the r^{th} resonance frequency, η_r is the r^{th} modal damping loss factor, and ω is the excitation frequency.

The k^{th} FRF shape is defined as the deflection of the structure in measured degrees of freedom due to a unit harmonic excitation at k^{th} degree of freedom.

$$\begin{aligned}
k^{\text{th}}\ \text{FRF shape at frequency}\ \omega\ &= \begin{Bmatrix} \alpha_{1k}(\omega) \\ \alpha_{2k}(\omega) \\ \vdots \\ \alpha_{nk}(\omega) \end{Bmatrix} \\
&= \begin{Bmatrix}
\dfrac{\phi_{11}\,\phi_{k1}}{\omega_1^2 - \omega^2 + i\eta_1\,\omega_1^2} + \dfrac{\phi_{12}\,\phi_{k2}}{\omega_2^2 - \omega^2 + i\eta_2\,\omega_2^2} + \cdots + \dfrac{\phi_{1n}\,\phi_{kn}}{\omega_n^2 - \omega^2 + i\eta_n\,\omega_n^2} \\
\dfrac{\phi_{21}\,\phi_{k2}}{\omega_1^2 - \omega^2 + i\eta_1\,\omega_1^2} + \dfrac{\phi_{22}\,\phi_{k2}}{\omega_2^2 - \omega^2 + i\eta_2\,\omega_2^2} + \cdots + \dfrac{\phi_{2n}\,\phi_{kn}}{\omega_n^2 - \omega^2 + i\eta_n\,\omega_n^2} \\
\vdots \\
\dfrac{\phi_{n1}\,\phi_{k1}}{\omega_1^2 - \omega^2 + i\eta_1\,\omega_1^2} + \dfrac{\phi_{n2}\,\phi_{k2}}{\omega_2^2 - \omega^2 + i\eta_2\,\omega_2^2} + \cdots + \dfrac{\phi_{nn}\,\phi_{kn}}{\omega_n^2 - \omega^2 + i\eta_n\,\omega_n^2}
\end{Bmatrix} \\
&= \frac{\phi_{k1}}{\omega_1^2 - \omega^2 + i\eta_1\,\omega_1^2}\ \{\phi\}_1 + \frac{\phi_{k2}}{\omega_2^2 - \omega^2 + i\eta_2\,\omega_2^2}\ \{\phi\}_2 + \cdots + \frac{\phi_{kn}}{\omega_n^2 - \omega^2 + i\eta_n\,\omega_n^2}\ \{\phi\}_n \\
&= \sum_{r=1}^{n} \frac{\phi_{kr}}{\omega_r^2 - \omega^2 + i\eta_r\,\omega_r^2}\ \{\phi\}_r
\end{aligned} \tag{6}$$

As can be seen from (6), FRF shapes are in tight relation with mode shapes and contain the modal information required for the damage detection. Damage is defined as the loss of stiffness in one or more elements of the structure. Mass disturbance due to damage is neglected.

4. APPLICATION OF POD IN STRUCTURAL DAMAGE DETECTION

In the modal-model-based damage detection methods, it is implicitly assumed that the modal data (*i.e.* mode shapes, resonant frequencies, and damping coefficients) represent the overall vibration behavior of the system in the frequency range under study. In this study, the response model of the structure is exploited and two approaches to FRF-based-damage detection via POD are proposed below.

4.1 Damage Detection Using Constructed Time Responses

Excitation of the structure with the force signal $f_k = F_k \sin \omega t$ at k^{th} DOF enforces j^{th} DOF to vibrate at the same frequency but at different levels of amplitude and phase, *i.e.* $x_j = X_j \sin(\omega t - \phi)$. According to Eq. (5), the response amplitude and phase are absolute and the phase of FRF between the DOFs i and j. At each exciting frequency, a response matrix is constructed whose rows and columns represent snapshots and measurement points, respectively, and the corresponding POM is calculated using Eqs. (2) or (3).

At the damaged node, the residual POM exhibits a local non-smoothness or curvature discontinuity. The GSM is implemented to quantify this behavior at each node. Figure 1 depicts a schematic of GSM. Line fitting through points before and after a specific node and subtracting line fitted prediction and the original

https://doi.org/10.1017/jmech.2011.17 Published online by Cambridge University Press

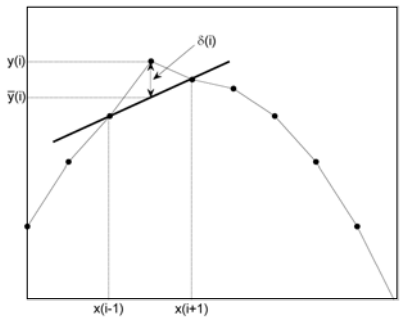


Fig. 1 Non-smoothness evaluation at node *i* via GSM

value comes to definition of index δ_i indicating relative degree of abnormality of node *i*. Some researchers used the cubic polynomial fitting through four data points. Despite the relatively higher accuracy of this method, it suffers from two drawbacks. Firstly, the damage detection at the boundaries of data intervals is fairly poor since the lack of data in these regions forces the use of extrapolation which is of lower accuracy. Secondly, its potential damage indication interval is wider compared to that of the linear GSM.

Making use of the fact that a single POM can capture the characteristics of FRF deflection shape at each excitation frequency, a damage detection algorithm is proposed in the following steps:

1. Measure a full row (or column) of FRF for both the intact and the damaged structures;
2. Calculate time histories of all DOFs at each frequency point using the FRF data as explained in Section 4.1;
3. Decompose the spatiotemporal data of step 2 for all frequency points via POD using either Eqs. (2) or (3);
4. Calculate a damage index based on the residual POM curvature or Gapped Smoothing Method (GSM) for each individual POM corresponding to each exciting frequency as explained in Section 4.1; and
5. Evaluate the damage region considering broadband GSM damage indices.

4.2 Damage Detection Using FRFs Directly

According to the second damage detection approach, spatio-spectral FRF shape data are directly decomposed via POD. The frequency content of the data severely affects the output POMs in this technique. It should be noted that FRF shapes at resonance frequencies coincide with the corresponding mode shapes. This method has several advantages over the mode shape analysis. Firstly, one can make use of all the data available in FRFs, *i.e.* data around anti-resonances. This property is useful when FRFs are estimated via $\hat{H}_1$ estimator in which a low input noise is assumed and the resonance data are noise polluted as a result. Secondly, FRF shape data include the effect of modes outside the test frequency range. FRF shapes showed to be combinations of mode shapes with some frequency dependent coefficients. If the FRF shapes are decomposed via POD in a specific frequency interval, basis vectors similar to neighboring mode shapes are usually dominant POMs. Making use of the residual POMs, *i.e.* the difference between the intact and damaged state POMs, the damaged zones correspond to the curvature discontinuity.

Based on the above observations, our second damage detection approach includes selecting a frequency interval, calculating the POMs of healthy and damaged structures via POD, and finding abnormal points in the residual POMs as potential damaged sites.

It should be noted that the frequency interval selected for damage detection strongly affects the results. Selection of resonance frequency range of analysis or test, results in approximate mode shapes as POMs, but the resulting POMs using non resonant intervals will be entirely different. This can provide more detailed information helping to localize structural damage. A detailed discussion will follow in the case studies below.

Both methods are evaluated using one numerical and two experimental case studies. In the second experimental case study, unlike the first one, a multiple damage scenario is considered to study the effectiveness of the method in such cases.

5. NUMERICAL CASE STUDY

A 0.9m length aluminum cantilever beam of the cross section $6.5 \times 25.5\text{mm}^2$ is discretized by 80 two dimensional beam elements each, having six degrees of freedom. Damage is simulated through reducing the thickness of element 20 by 7.7 percent. Dynamic responses have been calculated by applying a harmonic input force at node 21 in the frequency range of 0 to 500Hz with 0.1Hz frequency step for both intact and damaged structures. Five flexural modes are available in this frequency range. Natural frequencies of both intact and damaged beams are presented in Table 1.

Displacement data, except for the transverse vibrations, are discarded in order to simulate real test situations where all DOFs, especially the rotational ones, are difficult to measure.

5.1 Damage Detection Using Time Responses

At each frequency step, a 201×81 matrix is calculated whose columns and rows correspond to nodes and time steps, respectively. To avoid oversampling in the low frequency region and aliasing error at high frequencies, time steps of different lengths are selected for the frequencies. Time intervals are arranged so that 201 samples are gathered from two oscillation cycles at all frequencies. The POD is implemented for each data matrix and the dominant POM is calculated for both intact and damaged structures. The GSM is applied on the residual POM. By residual POM we mean the difference between intact and damaged state POMs at each frequency point. Figure 2 shows the normalized damage indices along the frequency range of analysis, which clearly indicates the damage in element 20.

https://doi.org/10.1017/jmech.2011.17 Published online by Cambridge University Press

Table 1 Natural frequencies of healthy and damaged beams in Hz

Mode	1	2	3	4	5
Frequency (intact beam)	6.58	41.37	115.62	226.58	374.34
Frequency (damaged beam)	6.53	41.03	114.99	226.03	373.12

One serious limitation in experimental approaches to damage detection is the limited number of measurement grid points. Adding more sensors for response recordings not only increases costs but disturbs structural mass distribution as well. To study the effectiveness of the proposed method in the case of coarse measurement grid points, the damage detection process is repeated with a reduced number of elements. Figures 3 to 5 show the results for 40, 20, and 10 elements used for damage localization. For better comparisons, damage indices are plotted along the dimensionless distance from the left end of the beam in Figs. 2 to 5. Damage location corresponds to the dimensionless length of $x/L = 0.245$, where L is the total length and x is the distance from the left end of the beam.

For 40-, 20-, and 9-element models, nodes 21, 6, and 3 carried the damage information, respectively. Damage in all the above mentioned cases was well located, as seen in Figs. 3 to 5. However, due to the lower number of data points, the damage zone width is increased as the number of elements decreases.

5.2 Damage Detection Using FRF Data

The second proposed approach was next implemented to localize the damage. Figures 6 to 9 depict the first three dominant POMs of the healthy and damaged beams along with their corresponding normalized residual POMs for four typical frequency intervals. As can be seen, a curvature discontinuity appears at the damaged site. Applying GSM to the residual POMs and averaging the indices through the first dominant basis vectors yields a damage indicative bar chart shown in Fig. 10 for various frequency intervals.

Figure 10 clearly shows the damaged zone on nodes 20 and 21, *i.e.* element 20. The four frequency intervals discussed for the damage localization are typical. One can try with arbitrary frequency intervals but it should be noted that the efficiency of the method varies when trying different frequency intervals. This is mainly because if the damage is located in a region where the curvature of basis vectors is of low amplitude, the damage is not typically detected properly; *i.e.*, different frequency intervals containing different basis vectors do not equally indicate the damage [25]. An efficient and automated technique for the selection of the proper frequency range as well as a statistical analysis will be investigated in future works.

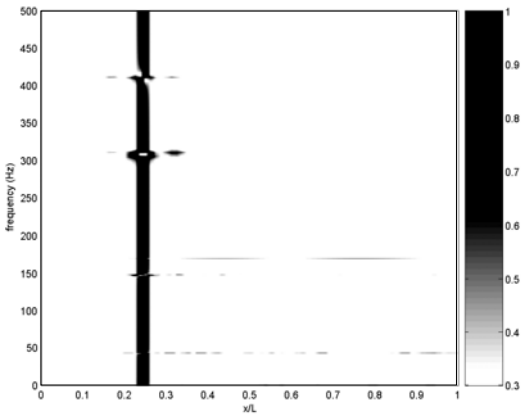


Fig. 2 Normalized damage indices over frequency range of analysis

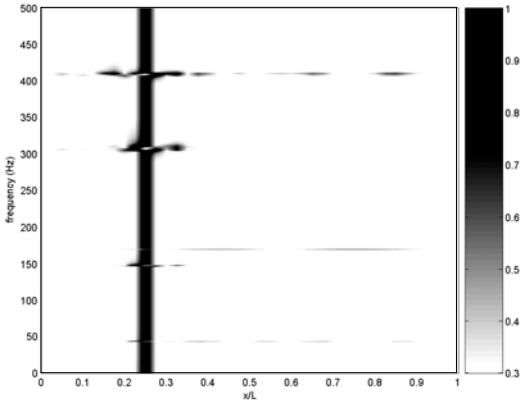


Fig. 3 Normalized damage indices using 40 elements

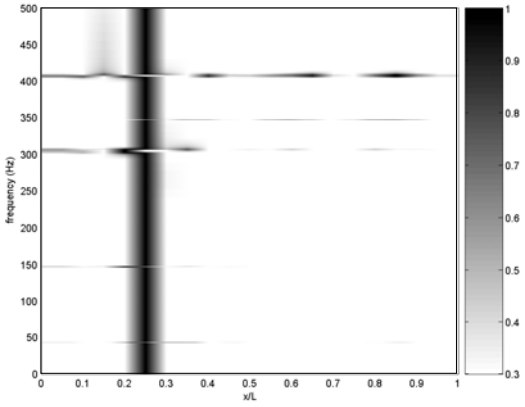


Fig. 4 Normalized damage indices using 20 elements

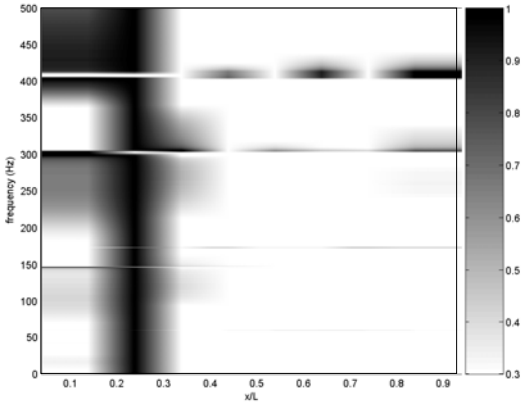


Fig. 5 Normalized damage indices using 9 elements

https://doi.org/10.1017/jmech.2011.17 Published online by Cambridge University Press

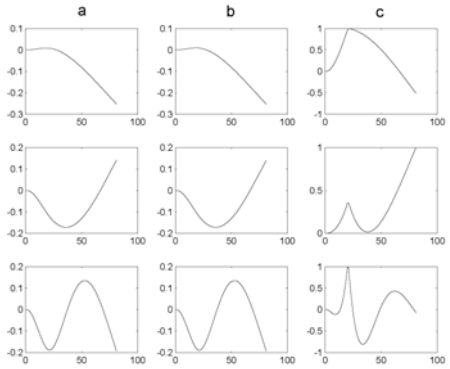


Fig. 6 POD of FRF shapes in 10-30Hz frequency interval: (a) the first three POMs of intact beam (b) the first three POMs of damaged beam (c) normalized corresponding residual POMs

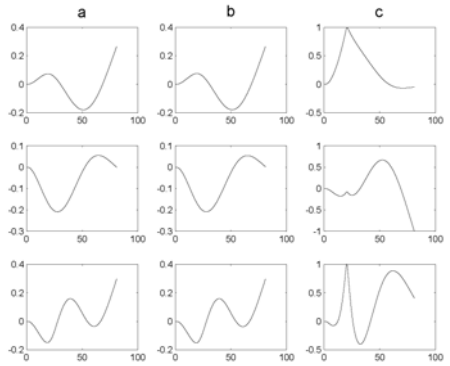


Fig. 7 POD of FRF shapes in 60-100Hz frequency interval: (a) the first three POMs of intact beam (b) the first three POMs of damaged beam (c) normalized corresponding residual POMs

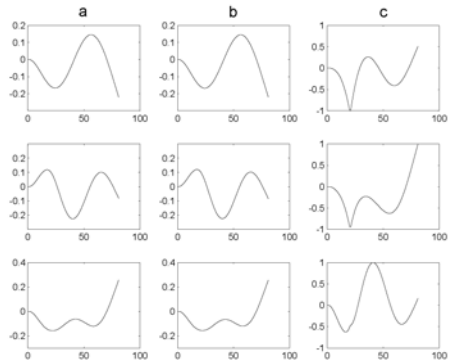


Fig. 8 POD of FRF shapes in 110-200Hz frequency interval: (a) the first three POMs of intact beam (b) the first three POMs of damaged beam (c) normalized corresponding residual POMs

6. EXPERIMENTAL CASE STUDY 1: THE SINGLE-DAMAGE CASE

To verify the proposed method from a practical point of view, modal test and analysis were carried out on a rectangular cross section aluminum beam. The test was carried out in the free-free condition by suspending

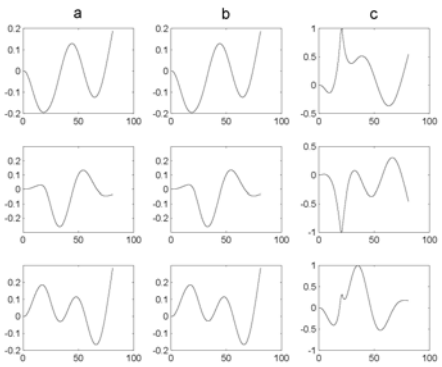


Fig. 9 POD of FRF shapes in 250-300Hz frequency interval: (a) the first three POMs of intact beam (b) the first three POMs of damaged beam (c) normalized corresponding residual POMs

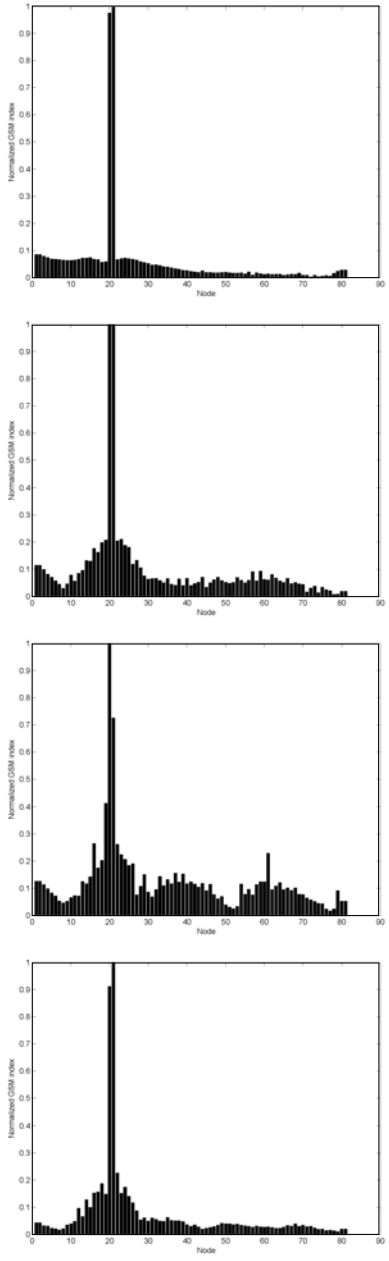


Fig. 10 Average of GSM indices of residual POMs for frequency range of 10-30Hz, 60-100Hz, 110-200Hz and 250-300Hz (from top to bottom)

https://doi.org/10.1017/jmech.2011.17 Published online by Cambridge University Press

the test object from some elastic bungees. The beam was of the cross section 50 × 25 millimeters and 800 millimeters length. Seventeen equally spaced measurement points were marked on the beam. The frequency range adopted was 0 to 1600Hz with frequency steps of 0.5Hz. A B&K 8202 hammer with a metal tip was used to excite the structure and the acceleration response was measured using a PCB 356B08 accelerometer in the vertical direction. The B&K Portable PULSE 3560D FFT analyzer was used to carry out and process the frequency response functions.

Damage was simulated through making an artificial slot of 10 millimeters deep over the width of the beam at node 7. The measured FRFs corresponding to various excitation points and the response at node 7 of the intact state beam are shown in Fig. 11. Resonance frequencies of the structure in both healthy and damaged states are shown in Table 2.

6.1 Damage Detection Using Time Responses

Application of the proposed POD-based method clearly revealed the damaged site. The results shown in Fig. 12 indicate that the damage occurred near node 7. There are some misleading frequency intervals in which the damage is not located correctly. Such results may be due to measurement noise and errors. Examination of the measured FRFs revealed that more than five FRFs were severely noise-contaminated in the frequency intervals of 200 ~ 300Hz and 650 ~ 800Hz in intact and damaged beams. Nevertheless, the overall damage localization seems to be satisfactory.

6.2 Damage Detection Using FRF Data

To verify the second proposed method experimentally, FRF shapes were directly decomposed via POD. Four frequency intervals were selected and the dominant POM basis vector in the healthy and damaged states were initially calculated in each case. Figure 13 shows the POMs and the corresponding residuals.

Residual curvature discontinuity in the damaged site is evident in Fig. 13. The associated GSM indices are shown in the form of bar charts for the considered frequency ranges in Fig. 14. Damage was successfully located in all considered frequency intervals. As mentioned earlier, one can use numerous frequency intervals to increase the reliability of damage detection by varying the center frequency and bandwidth.

7. EXPERIMENTAL CASE STUDY 2: MULTIPLE DAMAGE CASE

To study the effectiveness of the proposed method in multiple damage cases, a steel beam of 0.5 meter length and 2 × 1 centimeters rectangular cross section was considered for the second experimental case study in free boundary conditions. Eleven equally spaced measurement points were considered to attach lightweight Endevco 35A accelerometers. Analyzer and

Table 2 Natural frequencies of healthy and damaged aluminum beams in Hz

Mode	1	2	3
Frequency (intact beam)	201.7	549.6	1063.4
Frequency (damaged beam)	177.6	513.2	1054.4

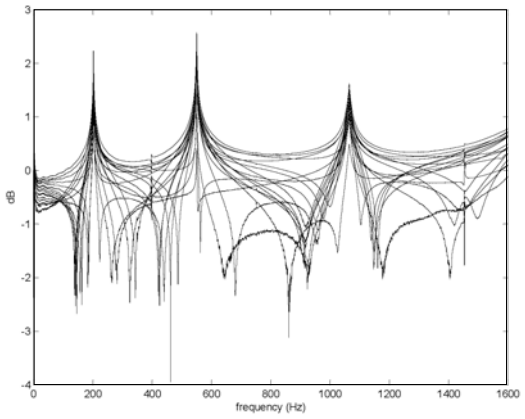


Fig. 11 Measured FRFs in undamaged case

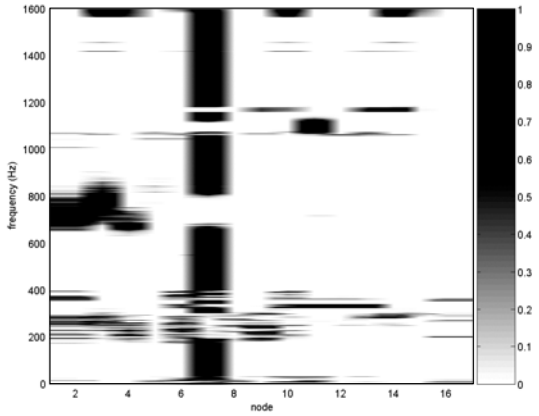


Fig. 12 Damage localization in the aluminum beam

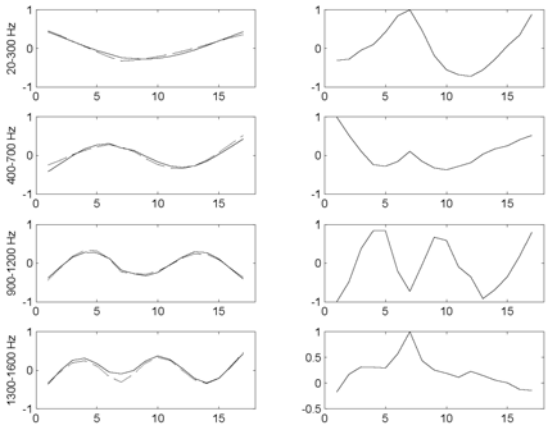


Fig. 13 First healthy (solid line) and damaged (dashed line) POMs (left column) and corresponding residual POMs (right column) of aluminum beam in frequency intervals 20-300Hz, 400-700Hz, 900-1200Hz and 1300-1600Hz (from top to down)

https://doi.org/10.1017/jmech.2011.17 Published online by Cambridge University Press

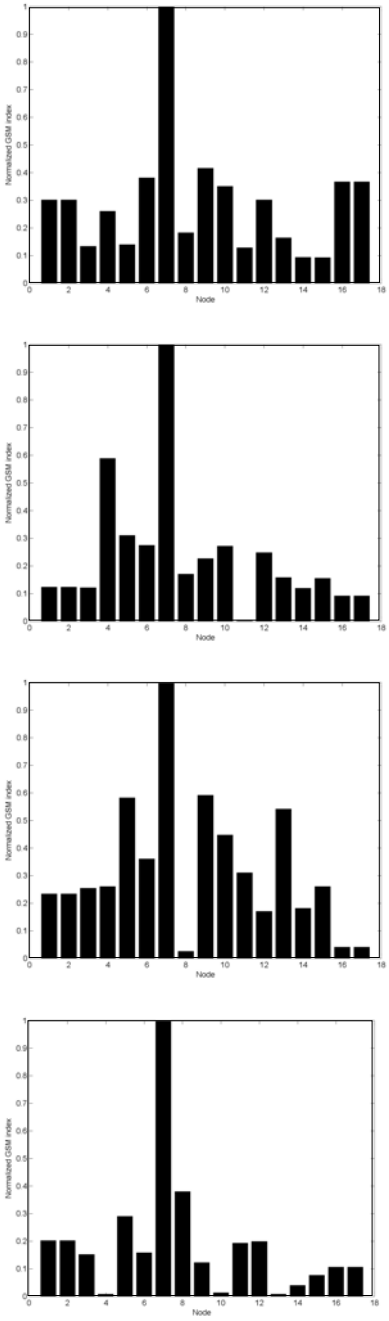


Fig. 14 Normalized GSM indices for frequency intervals 20 ~ 300Hz, 400 ~ 700Hz, 900 ~ 1200Hz and 1300 ~ 1600Hz (from top to bottom)

excitation equipment types were the same as those in the previous experimental case. Test data were acquired in the frequency range of 0 ~ 3200Hz with frequency increments of 0.5Hz. Figure 15 shows the test setup. Damage was modeled as two artificially slots of 0.4 centimeter depth at 10 and 25 centimeters from the left side of the beam corresponding to the experimental nodes 3 and 6.

All FRF matrix elements were measured in the frequency range of interest. Figure 16 shows FRFs gathered at node 1 due to excitation at all 11 grid points for the healthy case. Resonance frequencies of intact and damaged structures are presented in Table 3.



Fig. 15 The experimental test setup

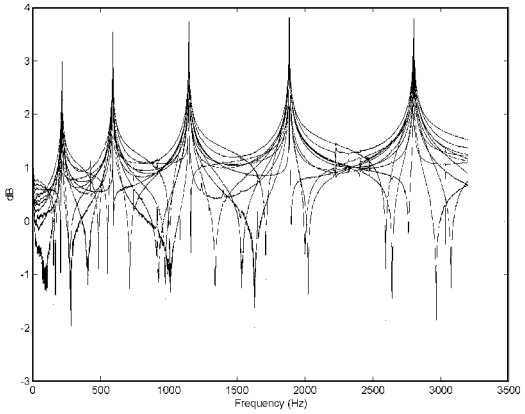


Fig. 16 Typical FRFs measured on the steel beam

Table 3 Natural frequencies of healthy and damaged steel beams in Hz

Mode	1	2	3	4	5
Frequency (intact beam)	214.2	588.0	1147.2	1885.3	2799.7
Frequency (damaged beam)	182.1	543.2	1032.9	1614.1	2475.8

7.1 Damage Detection Using Time Responses

The results of applying the proposed damage detection method are shown in Fig. 17. The damaged sites around nodes 3 and 6 are easily detectable from the Figure. Misleading results in some frequency portions are due to measurement noise and inadequate data.

7.2 Damage Detection Using FRF Data

The second proposed approach was also employed for the steel beam. Due to coarse measurement grid points, only one or two numerically meaningful POMs were implemented for damage detection. Figure 18 depicts POMs in the healthy and damaged states of the four frequency intervals selected and the corresponding residual POMs.

Figure 19 shows the normalized GSM indices for four frequency intervals selected. As can be seen from Fig. 19, the accuracy of method declines as the frequency range increases since FRF shape nodal points increase at higher frequencies and more measurement

https://doi.org/10.1017/jmech.2011.17 Published online by Cambridge University Press

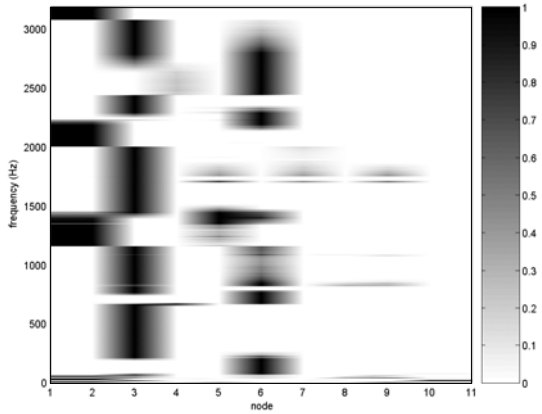


Fig. 17 Damage localization in the steel beam

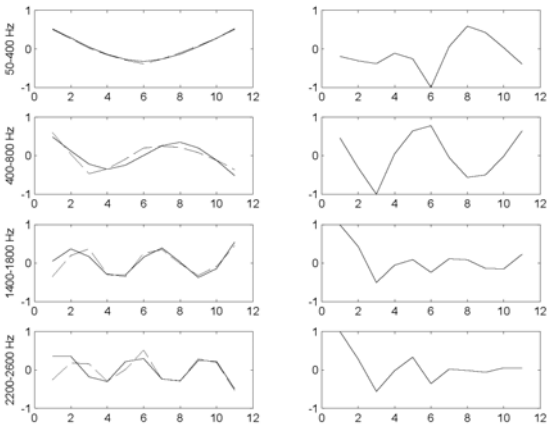


Fig. 18 First healthy (solid line) and damaged (dashed line) POMs (left column) and corresponding residual POMs (right column) of steel beam in frequency intervals 50 ~ 400Hz, 400 ~ 800Hz, 1400 ~ 1800Hz and 2200 ~ 2600Hz (from top to down)

points are needed to obtain signal details. In other words, if more accelerometers are attached to the beam, most of the misleading high-valued GSM indices in the non-damaged nodes decrease.

8. CONCLUSIONS

Two damage detection techniques were proposed based on the proper orthogonal decomposition using measured frequency response functions. The proposed methods are based on direct vibration test outputs and do not require modal analysis of data. Additionally, the proposed methods do not require any analytical models to localize the damage. In other words, only the experimental FRFs of the two intact and damaged structures are required. The methods were implemented in one numerical and two experimental case studies. The effects of measurement grid density were also investigated through the numerical case study. The overall results were satisfactory both for the single- and multiple-damage cases although loss of accuracy in damage localization was inevitable in some frequency portions due to experimental errors and data inadequacy.

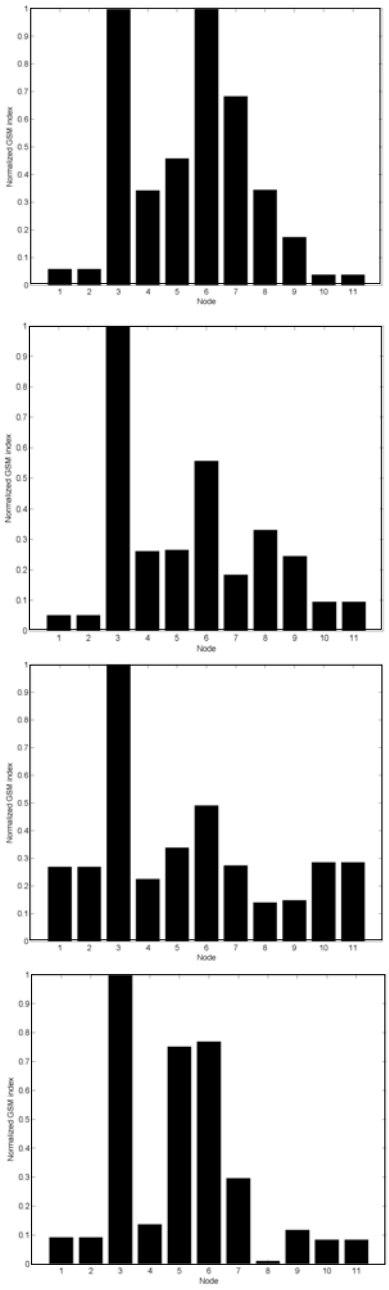


Fig. 19 Normalized GSM indices for frequency intervals 50 ~ 400Hz, 400 ~ 800Hz, 1400 ~ 1800Hz and 2200 ~ 2600Hz (from top to bottom)

REFERENCES

1. Sohn, H., Farrar, C. R., Hemez, F. M., Shunk, D. D., Stinemates, S. W., Nadler, B. R. and Czarnecki, J. J., "A Review of Structural Health Monitoring Literature From 1996-2001," Technical Report LA-13976-MS, Los Alamos National Laboratory Report, (2004).
2. Perera, R. and Ruiz, A., "Multi-Stage FE Updating Procedure for Damage Identification in Large Scale Structures Based on Multi-Objective Evolutionary Optimization," *Mechanical Systems and Signal Processing*, **22**, pp. 970–991 (2008).
3. Jaishi, B. and Ren, W. X., "Damage Detection by

https://doi.org/10.1017/jmech.2011.17 Published online by Cambridge University Press

Finite Element Model Updating Using Modal Flexibility Residual," *Journal of Sound and Vibration*, **290**, pp. 369–387 (2006).
4. Cawley, P. and Adams, R. D., "The Location of Defects in Structures from Measurements of Natural Frequencies," *Journal of Strain Analysis*, **14**, pp. 49–57 (1979).
5. West, W. M., "Illustration of the Use of Modal Assurance Criterion to Detect Structural Changes in an Orbiter Test Specimen," *Proceedings of the Air Force Conference on Aircraft Structural Integrity*, pp. 1–6 (1984).
6. Leiven, N. A. J. and Ewins, D. J., "Spatial Correlation of Mode Shapes, the Coordinate Modal Assurance Criterion (COMAC)," *Proceedings of the Sixth International Modal Analysis Conference*, **1**, pp. 690–695 (1988).
7. Lu, Q., Ren, G. and Zhao, Y., "Multiple Damage Location with Flexibility Curvature and Relative Frequency Change for Beam Structures," *Journal of Sound and Vibration*, **253**, pp. 1101–1114 (2002).
8. Pandy, A. K., Biswas, M. and Samman, M. M., "Damage Detection from Changes in Curvature Mode Shapes," *Journal of Sound and Vibration*, **145**, pp. 321–332 (1991).
9. Ewins, D. J., *Modal Testing: Theory, Practice and Application*, 2nd Ed., Research Studies Press, (2000).
10. Maia, N. M. M., Silva, J. M. M. and Sampaio, R. P. C., "Localization of Damage Using Curvature of the Frequency Response Functions," *XV International Modal Analysis Conference*, Orlando, USA, pp. 942–946 (1997).
11. Sampaio, R. P. C., Maia, N. M. M. and Silva, J. M. M., "Damage Detection Using the Frequency Response Function Curvature Method," *Journal of Sound and Vibration*, **226**, pp. 1029–1042 (1999).
12. Liu, X., Lieven, N. A. J. and Escamilla-Ambrosio, P. J., "Frequency Response Function Shape-Based Methods for Structural Damage Localization," *Mechanical Systems and Signal Processing*, **23**, pp. 1243–1259 (2009).
13. Adhikari, S. and Friswell, M. I., "Distributed Parameter Model Updating Using the Karhunen-Loeve Expansion," *Mechanical Systems and Signal Processing*, **24**, pp. 326–339 (2010).
14. Feeny, B. F. and Kappagantu, R., "On the Physical Interpretation of Proper Orthogonal Modes in Vibrations," *Journal of Sound and Vibration*, **211**, pp. 607–616 (1998).
15. Feeny, B. F. and Liang, Y., "Interpreting Proper Orthogonal Modes of Randomly Excited Vibration Systems," *Journal of Sound and Vibration*, **265**, pp. 953–966 (2003).
16. Chelidze, D. and Zhou, W., "Smooth Orthogonal Decomposition-Based Vibration Mode Identification," *Journal of Sound and Vibration,* **292**, pp. 461–473 (2006).
17. Galvanetto, U., Violaris, "Numerical Investigation of a New Damage Detection Method Based on Proper Orthogonal Decomposition," *Mechanical Systems and Signal Processing*, **21**, pp. 1346–1361 (2007).
18. Galvanetto, U., Surace, C. and Tassotti, A., "Structural Damage Detection Based on Proper Orthogonal Decomposition: Experimental Verification," *AIAA Journal*, **46**, pp. 1624–1630 (2008).
19. Trendafilova, I., Cartmellb, M. P. and Ostachowicz, W., "Vibration-Based Damage Detection in an Aircraft Wing Scaled Model Using Principal Component Analysis and Pattern Recognition," *Journal of Sound and Vibration*, **313**, pp. 560–566 (2008).
20. Chen, J. T., Chen, I. L. and Chen, K. H., "Treatment of Rank-Deficiency in Acoustics Using SVD," *Journal of Computational Acoustics*, **14**, pp. 157–183 (2006).
21. Wu, C. G., Liang, Y. C., Lin, W. Z., Lee, H. P. and Lim, S. P., "A Note on Equivalence of Proper Orthogonal Decomposition Methods," *Journal of Sound and Vibration*, **265**, pp. 1103–1110 (2003).
22. Kirby, M., *Geometric Data Analysis: An Empirical Approach to Dimensionality Reduction and the Study of Patterns,* John Wiley, U.S.A. (2001).
23. Kerschen, G. and Golinval, J. C., "Physical Interpretation of the Proper Orthogonal Modes Using the Singular Value Decomposition," *Journal of Sound and Vibration*, **249**, pp. 849–865 (2002).
24. He, J. and Fu, Z. F., *Modal Analysis*, Butterworth-Heinemann press (2001).
25. Salehi, M., Ziaei-Rad, S. and Ghayour, M., "A Structural Damage Localization Method Based on Dynamically Measured Flexibility Matrix," *Proceedings of 8th Aerospace Conference*, Shahinshahr, Iran (2009).

(Manuscript received March 4, 2010,
accepted for publication May 31, 2010.)

https://doi.org/10.1017/jmech.2011.17 Published online by Cambridge University Press